Configuration mixing in ^{56}Co and ^{46}Sc using $(\vec{d},\alpha)$ reactions

E. R. Crosson and E. J. Ludwig
University of North Carolina at Chapel Hill, North Carolina 27599
and Triangle Universities Nuclear Laboratory, Durham, North Carolina 27708

M. Bisenberger, R. Hertenberger, D. Hofer, H. Kader, P. Schiemenz, and G. Graw
Sektion Physik, Universität München, 8046 Garching, Germany

A. M. Eiró and F. D. Santos
Departamento de Fisica and Centro de Física Nuclear da Universidade de Lisboa, 1700 Lisboa, Portugal

B. A. Brown
Michigan State University, East Lansing, Michigan 48824
(Received 1 June 1993)

Two-nucleon spectroscopic amplitudes are investigated using cross-section measurements and tensor analyzing powers for the ^{58}Ni$(\vec{d},\alpha)^{56}$Co and ^{48}Ti$(\vec{d},\alpha)^{46}$Sc reactions. Angular distributions of cross sections, and analyzing powers A_y, A_{xx}, and A_{yy}, were measured in steps of 5° from 10° to 65° at a bombarding energy of 22 MeV. Data were analyzed using full finite-range DWBA calculations including a realistic α-particle wave function. The L-mixing ratios for several strong unnatural-parity transitions have been determined from comparison of calculations with analyzing power data. These ratios are compared to predictions of shell-model calculations to deduce predominant two-nucleon configurations.

PACS number(s): 21.10.Jx, 24.70.+s, 25.45.Hi, 27.40.+z

I. INTRODUCTION

Two-nucleon transfer reactions have long been recognized as a valuable tool for spectroscopic studies [1]. Among these, the (d,α) reaction is especially interesting since it can be used to probe neutron-proton correlations within complex nuclei. This reaction involves the transfer of a spin-1 neutron-proton cluster, and hence, for unnatural-parity transitions of a unique J transfer, it is possible to have a mixing of transition amplitudes with different orbital angular momentum $L=J\pm1$. Nuclear structure studies of n-p hole states involving analysis of differential cross-section data for a given transition can identify only the predominant orbital angular momentum of transferred clusters, while vector analyzing powers (VAP's) are relatively insensitive [2] to this mixing. Tensor analyzing power (TAP) measurements, however, have been shown to be quite sensitive [2] to the magnitude and sign of the L-mixing ratio R. The investigation [2] of several low-lying states populated in the ^{89}Y$(\mathbf{d},\alpha)^{87}$Sr reaction has been successful in suggesting the sign and strength of the spectroscopic amplitudes from TAP angular distributions. Studies [3] of ^{36,38}Ar$(\mathbf{d},\alpha)^{34,36}$Cl have additionally shown agreement between predictions of shell-model calculations for the sd-shell and experimentally determined phases of the L-mixing ratios as well as their magnitude in certain cases. For fp-shell nuclei studied as part of the present work, the spectroscopic amplitudes can now be predicted by shell-model calculations which include $1f_{7/2}$, $1f_{5/2}$, $2p_{3/2}$, and $2p_{1/2}$ active orbitals. These calculations include a mass-dependent effective interaction.

The TAP angular distributions are sensitive to the presence of a D-state component of the α particle formed by the pickup of a target deuteron by the projectile [4,5]. Realistic α-particle wave functions [6] corresponding to S- and D-state deuteron-deuteron overlaps $\langle dd|\alpha\rangle$ have recently been employed in exact finite-range distorted-wave Born approximation (DWBA) calculations of the ^{58}Ni$(\mathbf{d},\alpha)^{56}$Co reaction to produce satisfactory agreement with the TAP angular distributions [4]. Since calculations omitting the D state produce a poor description of TAP data [7], the inclusion of a D-state wave function is essential to the extraction of spectroscopic information from the observed mixing ratios in this reaction.

It is the goal of the present work to extract R from measured cross sections and tensor analyzing powers in (d,α) reactions using exact finite-range DWBA calculations which include overlap functions generated from realistic α-particle wave functions. From these ratios, the predominant configurations involved in the two-nucleon pickup process are suggested in some cases. Future shell-model calculations can then be refined based on the L-mixing ratios obtained. These studies provide valence-nucleon orbital information of the type that CEBAF may be able to obtain for deeper-lying orbitals probed in complex $(e,e'np)$ experiments.

II. EXPERIMENTAL PROCEDURE

The cross-section, VAP, and TAP angular distribution data for the ^{58}Ni$(\mathbf{d},\alpha)^{56}$Co and ^{48}Ti$(\mathbf{d},\alpha)^{46}$Sc reactions were measured at the Munich HVEC-MP tandem accelerator laboratory at a deuteron energy of 22 MeV.

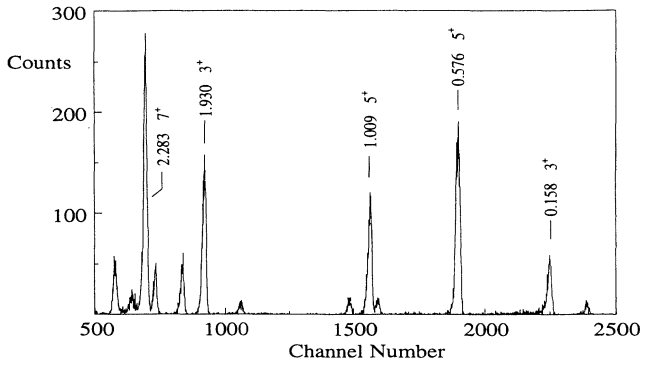

FIG. 1. Spectrum of the ^{58}Ni(d,α)^{56}Co reaction at $\theta=10°$ with residual nucleus excitation energies from 0 to 2.5 MeV. Excitation energies are in MeV. The deuteron energy is 22 MeV.

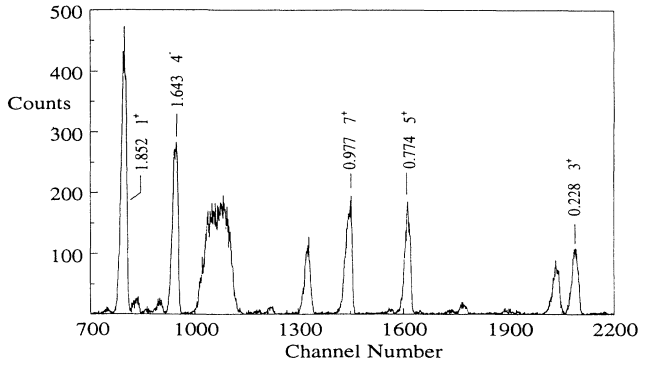

FIG. 2. Spectrum of the ^{48}Ti(d,α)^{46}Sc reaction at $\theta=10°$ with residual nucleus excitation energies from 0 to 2.0 MeV. Excitation energies are in MeV. The deuteron energy is 22 MeV.

The polarized beam of deuterons was produced with the improved Lamb-shift polarized ion source [8] operated in a spin-filter mode. Using separate magnetic substates $m=+1$, $m=0$, and $m=-1$, observables were obtained using the standardized three-state measurement scheme [9]. Beam polarization was determined by periodic quench-ratio-type measurements [9] with an absolute error estimated to be 10%. The orientation of the beam polarization axis was adjusted using a Wien filter to be perpendicular to the reaction plane for A_{yy} measurements or in the reaction plane for A_{xx} determinations. The α particles were detected using a Q3D magnetic spectrograph with a focal-plane detector system [10] that uses kinematic corrections to achieve a resolution of 12 keV full width at half maximum (FWHM) at the full spectrograph acceptance of 11 msr.

Targets of 40 and 154 μg/cm^2 ^{58}Ni were produced from 99.9% enriched isotope deposited on 11-μg/cm^2 carbon foils using standard electron-gun evaporation techniques [11]. The titanium target was a 260-μg/cm^2 self-supporting foil 99.2% enriched in ^{48}Ti and produced by standard rolled-foil techniques [11]. The targets were relatively free of contaminants, as shown by the spectra in Figs. 1 and 2. Target thicknesses were determined by a weight measurement and by comparing forward-angle α-particle elastic scattering with calculated Rutherford-scattering yields. The target thicknesses were determined to an accuracy of 10%.

Most of the ^{58}Ni(d,α)^{56}Co data were taken using the 154-μg/cm^2 ^{58}Ni target. The energy loss of exiting α particles was $\sim$24 keV in this target, and when energy-loss effects were combined with spectrometer resolution an overall spectrum resolution of 27 keV FWHM was obtained. Data taken with the 40-μg/cm^2 ^{58}Ni target yielded an overall resolution of $\sim$14 keV. Because of the low cross section for some states, this target proved too thin to use through most of the experiment and mainly served as a means of examining possible contaminant peaks or doublets in the spectra. The energy bite of the 1.2-m-long focal-plane detector of the spectrograph was 2.5 MeV when adjusted for 28-MeV α particles. This allowed about 11 states with excitation energies in ^{56}Co below 2.4 MeV to be cleanly resolved. The resolution of the ^{48}Ti(d,α)^{46}Sc spectrum, shown in Fig. 2, is $\sim$35 keV, resulting from the use of the 260-μg/cm^2 target during most of the experiment. A total of about nine states below 2.4-MeV excitation in ^{46}Sc were sufficiently populated so that angular distributions could be obtained [12]. In Table I we list the peak differential cross section for states resolved in this study to provide an indication of the relative transition probabilities.

TABLE I. Peak differential cross section for states resolved in this study.

^{58}Ni(d,α)^{56}Co			^{48}Ti(d,α)^{46}Sc		
E_{ex} (keV)	J^π	σ_{peak} (μb/sr)	E_{ex} (keV)	J^π	σ_{peak} (μb/sr)
0	4^+	14	0	4^+	22
158	3^+	100	52	6^+	21
576	5^+	200	228	3^+	97
970	2^+	11	585	3^-	30
1009	5^+	120	774	5^+	142
1114	3^+	22	977	7^+	134
1720	1^+	14	1643	4^-	253
1930	3^+	190	1852	1^+	295
2060	2^+	48			
2225	2^+	39			
2283	7^+	430			

III. ANALYSIS

Cross-section and TAP angular distribution data were compared to exact finite-range DWBA calculations using the code TWOFNR [13]. The transition amplitudes for direct one-step $A(d,\alpha)B$ reactions can be expressed as

$$T_{\mathrm{DWBA}}=\int d\mathbf{r}_d \int d\mathbf{r}_\alpha \chi_\alpha^{*(-)}(\mathbf{r}_\alpha) \times\langle B,\alpha|V_{dd}|A,d\rangle\chi_d^{(+)}(\mathbf{r}_d) , \quad (1)$$

where χ_d and χ_α are optical-model wave functions corresponding to the entrance and exit channels and V_{dd} is the interaction potential between the two deuterons forming the α particle. The dependence on the ^{4}He internal structure is contained in the form factor

$$F(\mathbf{r})=\langle\phi_d\phi_d|V_{dd}|\phi_\alpha\rangle , \quad (2)$$

where ϕ_d,ϕ_α are the ^{2}H,^{4}He bound-state wave functions, respectively. Using the ^{4}He Schrödinger equation, we can write

$$F(\mathbf{r})=-\left[B_\alpha-2B_d-\frac{\hbar^2}{2\mu}\nabla^2\right]G(\mathbf{r}) , \quad (3)$$

where B_α and B_d are the binding energy of the α particle and the deuteron, respectively, and

$$G(\mathbf{r})=\langle\phi_d\phi_d|\phi_\alpha\rangle =\tfrac{1}{2}(-1)^{\sigma_1}\sum_{L'=0,2}(LM1\sigma_1|1-\sigma_2)u_{L'}(r)Y_L^M(\hat{\mathbf{r}}) \quad (4)$$

is the overlap function that describes the two-deuteron configuration in ^{4}He, σ_1 and σ_2 are the spin projections of the deuterons, and $u_{L'}(r)$ the radial wave functions. For the present work, the S- and D-state components of the overlap in configuration space were calculated [4] from the momentum distributions in ^{4}He obtained by Schiavilla, Pandharipande, and Wiringa [6]. It should be emphasized that these wave functions, containing the full complexity of N-N interactions, are at present the best available predictions of the projected α-particle wave functions onto two deuterons. Previous finite-range analyses of (d,α) reactions were performed [14,15] using the phenomenological form factor generated in a Woods-Saxon well with well depths adjusted to yield the correct binding energy of an alpha in the $\alpha=d+d$ system.

The two-particle structure of the target in the transition amplitude can be described microscopically in the framework of shell-model calculations. For a final state corresponding to a transfer of spin J and isospin T, the overlap between the target A and the residual nucleus B is described in terms of the wave function of individual nucleons Ψ_{ji} from configuration $\eta(j_1,j_2)$ weighted with a generalized two-nucleon spectroscopic amplitude $\beta(\eta,J,T)$ by

$$\langle B|A\rangle_{J,T}=\sum_\eta\beta(\eta,J,T)[\psi_{j_1}(\mathbf{r}_1,s_1)\otimes\psi_{j_2}(\mathbf{r}_2,s_2)]_{J,T} . \quad (5)$$

Alternatively, one can use a cluster model to account for the dynamics of the reaction, assuming the transfer of a particle of mass 2 and spin 1 with wave function $\phi_{l_1}(\mathbf{r})$ and express $\langle B|A\rangle$ in terms of the amplitudes $G(L,J)$ corresponding to the allowed L values,

$$\langle B|A\rangle_{J,T}=\sum_L G(L,J)[\psi_{LS}(\mathbf{R})\otimes\phi_{l_1}(\mathbf{r})]_{J,T} . \quad (6)$$

The advantage of the latter procedure, where usually we consider only $l=0$ terms, is to describe correctly the asymptotic behavior of the tail of the relative wave function $\psi_{LS}(\mathbf{R})$ for the motion of the cluster in the target. In the present work, $\psi_{LS}(\mathbf{R})$ was generated in a Woods-Saxon potential. This procedure is crucial for reactions at our energies, which tend to take place at the surface of the nucleus.

In the particular case of harmonic oscillator wave functions, the basis states of these two expansions are exactly correlated by the Talmi-Moshinsky transformation

$$[\psi_{j_1}(\mathbf{r}_1,s_1)\otimes\psi_{j_2}(\mathbf{r}_2,s_2)]_{J,T} =\sum_L G_{LSJ}(\eta)[\psi_{LS}(\mathbf{R})\otimes\phi_{l_1}(\mathbf{r})]_{J,T} , \quad (7)$$

where the structure amplitudes $G_{LSJ}(\eta)$ include the symmetrized LS-JJ coupling coefficient [16]. Assuming that Eq. (7) is a reliable approximation for the Woods-Saxon prescription, one may then use the values of $G(L,J)$ obtained from the analysis of experimental data and compare with the value obtained using the shell-model amplitudes $\beta(\eta,J,T)$, by summing up over the allowed configurations

$$G(L,J)=\sum_\eta G_{LSJ}(\eta)\beta(\eta,J,T) . \quad (8)$$

In the case of unnatural-parity transitions, the ratio

$$R=\frac{G(L=J+1,J)}{G(L=J-1,J)} \quad (9)$$

is a measure of the L mixing. If we consider a specific configuration η, we can calculate $R(\eta)$. For a pure configuration, the mixing ratio is a purely geometrical quantity and may be taken as a guide to identify simple model states or determine weak admixtures.

The entrance- and exit-channel distorted waves were parametrized using Woods-Saxon optical-model potentials (OMP's) and are identical to those used in Ref. [4]. The DWBA calculations used in this work are therefore consistent with those obtained for the strong (and unmixed in L) 7^+ levels in ^{56}Co at 2.283 MeV and ^{46}Sc at 0.977 MeV. The deuteron OMP's for ^{58}Ni$(d,\alpha)^{56}$Co and ^{48}Ti$(d,\alpha)^{46}$Sc were obtained from the global parametrization of Daehnick, Childs, and Vrcelj [17], except that the real well depth was reduced by 2% to improve the description of $(\mathbf{d},\alpha)$ vector analyzing powers, as described in Ref. [4]. Exit-channel OMP parameters for ^{58}Ni$(d,\alpha)^{56}$Co and ^{48}Ti$(d,\alpha)^{46}$Sc were generated by fitting angular distribution data [12] measured at TUNL for ^{59}Co$(\alpha,\alpha)^{59}$Co and ^{58}Ni$(\alpha,\alpha)^{58}$Ni at energies of 18.5, 22.5, and 24 MeV and for ^{50}Ti$(\alpha,\alpha)^{50}$Ti at 20 MeV. The analysis of these data was designed to obtain the best set of OMP parameters consistent with folding-model calculations [18] and with fits to higher-energy data by Goldberg, Smith, and Burdzik [19]. Systematic tests were

made of the sensitivity of $(\mathbf{d},\alpha)$ observables to changes in both entrance- and exit-channel OMP parameters consistent with maintaining good agreement with elastic-scattering channels. It was found that such changes could affect cross section and VAP predictions; however, relatively small changes in TAP predictions were observed [20].

IV. RESULTS AND DISCUSSION

To establish L mixing in these (d,α) reactions, only the strong transitions to the residual nuclei ^{56}Co and ^{46}Sc were analyzed, since the reaction mechanism for weaker levels is more likely to be complicated by the presence of multistep processes. Daehnick *et al.* [21] have pointed out that processes such as $(d,t)(t,\alpha)$ and $(d,^3\mathrm{He})(^3\mathrm{He},\alpha)$ can strongly influence the reaction yield even for strong transitions. The contribution of such two-step processes has been estimated [20] for the strong transition to the 7^+ level at 2.283 MeV in ^{56}Co, measured as part of the present work, despite the lack of input as to the strength of the relevant single-nucleon transfer data. It was found that two-step contributions affected TAP predictions for A_{xx} at a level comparable to that produced by changes in OMP parameters and that slightly larger changes were observed for A_{yy} and A_y. The good agreement obtained between experimental data and calculations of TAP's, including only a direct amplitude provides additional justification for our neglect of two-step processes in the present work.

The curves shown with data in Figs. 3 and 4 result from exact finite-range DWBA calculations employing realistic S- and D-overlap functions corresponding to the Argonne interaction [6] for the α particle. For the target nucleus, the neutron and proton were assumed to be transferred as a cluster, with a wave function generated in a Woods-Saxon well consistent with the separation energy of a deuteron in the residual nucleus. Comparisons to cross-section data are adjusted to match the cross-section peak. The solid curves correspond to the average value of L mixing which provides the best fit to the two TAP angular distributions. This fit was generated by varying R in steps of 0.1 from -1.0 to 1.0 to minimize χ^2 where

$$\chi^2=\Sigma_i[(A_{\mathrm{th}}-A_{\mathrm{ex}})^2/\Delta A_{\mathrm{ex}}^2]_i \ .$$

Here A_{th} and A_{ex} are the predicted and experimental analyzing powers for A_{xx} and A_{yy}, while ΔA_{ex} is the error in the analyzing powers. Plots of χ^2 versus R shown for certain L-mixed transitions are presented in Fig. 5. A very interesting feature of these plots is the presence of a pronounced minimum, almost at the same value of R for both observables in each transition, allowing the extraction of a best-fit value for the mixing ratio. The cross section and VAP χ^2 were also calculated, using the same procedure as above. Typically, in the case of VAP's there is little sensitivity to R, while the results for the cross section can be used to exclude certain ranges of R as shown in Fig. 6. Shell-model predictions were made for low-lying states using the code OXBASH [22]. The calculation was restricted to the fp shell, and the active orbitals included were $1f_{7/2}$, $1f_{5/2}$, $2p_{3/2}$, and $2p_{1/2}$, leading to ten possible two-nucleon configurations:

$$\eta_1=\pi(1f_{7/2})\nu(f_{7/2}) \ , \quad \eta_2=\pi(1f_{7/2})\nu(2p_{3/2}) \ ,$$
$$\eta_3=\pi(2p_{3/2})\nu(2p_{3/2}) \ , \quad \eta_4=\pi(1f_{7/2})\nu(1f_{5/2}) \ ,$$
$$\eta_5=\pi(2p_{3/2})\nu(1f_{5/2}) \ , \quad \eta_6=\pi(1f_{5/2})\nu(1f_{5/2}) \ ,$$
$$\eta_7=\pi(1f_{7/2})\nu(2p_{1/2}) \ , \quad \eta_8=\pi(1f_{5/2})\nu(2p_{1/2}) \ ,$$
$$\eta_9=\pi(2p_{1/2})\nu(2p_{1/2}) \ , \quad \eta_{10}=\pi(2p_{3/2})\nu(2p_{1/2}) \ .$$

The two-particle spectroscopic amplitudes were calculated in a model space which allowed for zero, one, or two particles to be excited from the $1f_{7/2}$ orbital to any of the $2p_{3/2}$, $1f_{5/2}$, or $2p_{1/2}$ orbitals. For ^{48}Ti and ^{46}Sc, the calculations were performed with the FPD6 effective interaction of Ref. [23], while for ^{58}Ni and ^{56}Co, the new interaction of Van der Merwe, Richter, and Brown [24] was used.

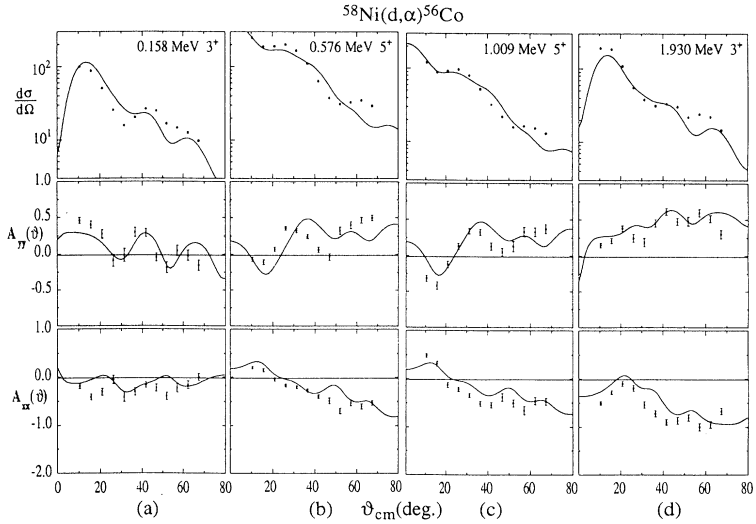

FIG. 3. Angular distributions of the cross section $(d\sigma/d\Omega)$ in μb/sr, A_{yy} and A_{xx}, at $E_d=22$ MeV for the ^{58}Ni$(\mathbf{d},\alpha)^{56}$Co to (a) the 3^+ state of ^{56}Co at $E_x=0.158$ MeV, (b) the 5^+ state of ^{56}Co at $E_x=0.576$ MeV, (c) the 5^+ state of ^{56}Co at $E_x=1.009$ MeV, and (d) the 3^+ state of ^{56}Co at $E_x=1.930$ MeV. The solid curves are DWBA calculations using realistic $\langle dd|\alpha\rangle$ form factors generated with the Argonne potential and correspond to the best-fit value for the L-mixing ratio, as described in the text. The DWBA calculation of $d\sigma/d\Omega$ is normalized to the data.

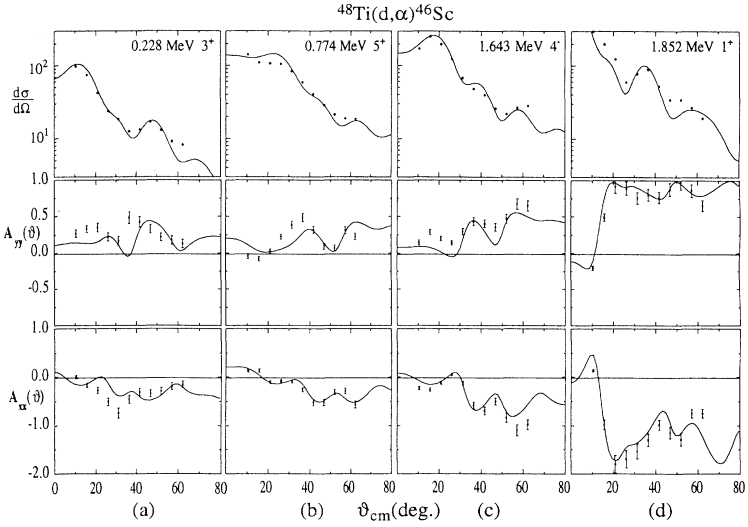

FIG. 4. Angular distributions of the cross section ($d\sigma/d\Omega$) in μb/sr, A_{yy} and A_{xx}, at $E_d=22$ MeV for the ^{48}Ti(**d**,α)^{46}Sc to (a) the 3^+ state of ^{46}Sc at $E_x=0.228$ MeV, (b) the 5^+ state of ^{46}Sc at $E_x=0.774$ MeV, (c) the 4^- state of ^{46}Sc at $E_x=1.643$ MeV and, (d) the 1^+ state of ^{46}Sc at $E_x=1.852$ MeV. The curves are DWBA calculations using realistic $\langle dd|\alpha\rangle$ form factors generated with the Argonne potential and correspond to the best-fit value for the L-mixing ratio, as described in the text. The DWBA calculation of $d\sigma/d\Omega$ is normalized to the data.

A. L-mixed transitions in the ^{58}Ni(d,α)^{56}Co reaction

Figure 3 shows the measured angular distributions of the cross section, A_{xx} and A_{yy}, for low-lying levels in ^{56}Co, obtained at an incident energy of 22 MeV. Excitation energies, spins, and parities of these levels were obtained from Ref. [25].

1. 3^+ level at 0.158 MeV

From the data, shown in Fig. 3(a), we see that the cross section peaks at $\theta<20°$, indicating dominance of the $L=2$ transfer. The best fits to A_{xx} and A_{yy}, having a sharp minimum in χ^2 for both observables, were obtained for $R=G(4,3)/G(2,3)=0.1$, as seen in Fig. 5. This value for the mixing is compatible with previous analyses of cross-section [26] and VAP [27] measurements for this transition, which showed it to be strongly $L=2$. Similar to the behavior that can be observed in Fig. 6, the cross section χ^2, excluding the region with $|R|>1$, shows little sensitivity and minimizes at R larger than 0.1.

The shell model predicts this relatively strong transition to proceed predominantly by the pickup of the η_2 configuration. If we assume only η_2 pickup, we obtain for the mixing ratio $R(\eta_2)=-0.32$. Of the other configurations expected to contribute with some significance to this transfer, η_1 and η_3, the strong presence of either can yield the small positive ratio indicated by the χ^2 minimization. Because of the large number of allowed configurations potentially involved in this transfer, we are unable to make unique determinations of the strength and sign of the spectroscopic amplitudes. When there are no more than two $G(L,J)$ amplitudes allowed, as is always the case for $J^\pi=0^+$ target nuclei, the extraction of the spectroscopic amplitudes may be possible when only two configurations contribute significantly, as has been shown in the analysis of the ^{89}Y(d,α)^{87}Sr reaction [2]. Shell-model calculations including all the allowed configurations predict η_2 to dominate and a value for $R=-0.4$ which does not agree well with the value extracted from TAP data. Values of R extracted from fits to TAP angular distributions are presented in Table II along with shell-model predictions.

2. 5^+ level at 0.576 MeV

Aside from the 7^+ level at 2.283 MeV, the reaction at this energy populates this level more strongly than any other in ^{56}Co. Previous studies of this reaction using cross-section measurements [26] and VAP's [27] have

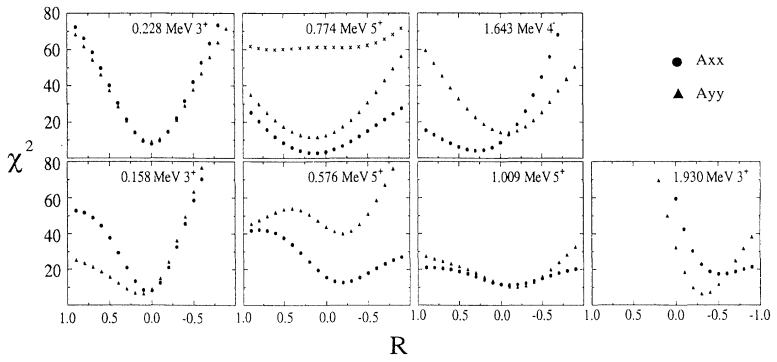

FIG. 5. χ^2 values are presented as a function of the L-mixing ratio R for A_{yy} (triangles) and A_{xx} (dots). The crosses shown in the figure for the 0.774-MeV state in ^{46}Sc indicate χ^2 variations with R for A_y data. The upper plots correspond to ^{48}Ti(**d**,α)^{46}Sc transitions and the lower plots to ^{58}Ni(**d**,α)^{56}Co transitions.

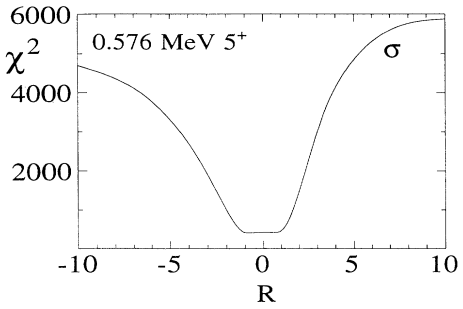

FIG. 6. Variations of χ^2 with R for cross-section data corresponding to the 5^+ state of ^{56}Co at $E_x = 0.576$ MeV.

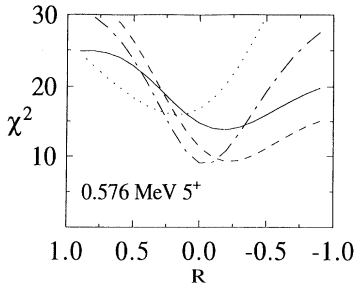

FIG. 7. Variations of χ^2 with R for A_{xx} data corresponding to the 5^+ state of ^{56}Co at $E_x = 0.576$ MeV. The solid curve was generated using our standard deuteron cluster geometry in the heavy system and α OMP's, the dashed curve using a cluster geometry which produced the best fit to A_{xx} data and the same α OMP's. In the dotted and dot-dashed curves, we kept the same cluster geometry for the heavy system as in the solid curve, and we changed the α OMP's by using a real-well depth decreased by 3% (dotted curve) and a real-well depth increased by 3% (dot-dashed curve).

identified this transition as a predominant $L = 4$ transfer, although there is some evidence for the presence of $L = 6$. The χ^2 minimizations for A_{xx} and A_{yy} data, shown in Fig. 5, indicate that $R = G(6,5)/G(4,5) = -0.2$ provides the most acceptable fit to both of these angular distributions, presented in Fig. 3(b). Shell-model calculations performed as part of the present work predict the dominant pickup of η_2 with $R = -0.15$ in excellent agreement with the value extracted from data.

We have varied the geometry of the Woods-Saxon potential that generates the deuteron cluster wave function in the target and the real-well depth of the α OMP's to test their influence on the position of the χ^2 minimum. Results obtained by varying R with different potential values are shown in Fig. 7. We can see that the position of the χ^2 minimum is quite insensitive to the variations in the geometry, and although they show some sensitivity to the different α OMP's the variations in the values of R are not large. These variations provide an indication of the uncertainty in R values that can be extracted using this method. In order to show the sensitivity of R to the cross-section angular distribution data, we show in Fig. 6 the variation of χ^2 with R for this state. We can see little variation in χ^2 over a range of ± 1.0 with great variation beyond that range. This is characteristic of most of the analyses of cross-section data made to date and suggests that angular distributions of the analyzing powers A_{xx} and A_{yy} are significantly better indicators of the magnitude of orbital angular momentum mixing than the commonly used cross-section distributions for this reaction at this energy. Cross-section data can, however, be a good indicator of the magnitude of R in certain cases, as discussed in Sec. IV B 4.

3. 5^+ state at 1.009 MeV

Transitions to this state have quite similar angular distributions to those of the 5^+ state at 0.576 MeV for the cross section and TAP's, as seen in Fig. 3(c). The population of this state is, therefore, expected to proceed mainly by $L = 4$ transfer, suggesting that the states have similar structure. Previous determinations based on the cross section [26] and VAP's [27] show a strong $L = 4$ transfer. The values of $R = G(6,5)/G(4,5)$ obtained from fits to A_{xx} and A_{yy} data are -0.1 and -0.2, respectively.

Shell-model calculations performed as part of the present work predict a dominant pickup of η_2 leading to $R = 0.36$. The similarity to the results for the 0.576-MeV state suggests an increased η_2 amplitude over that predicted by the present shell-model calculations.

4. 3^+ state at 1.930 MeV

Unlike the case of the two 5^+ states, angular distributions measured for this 3^+ state do not appear similar to those for the 3^+ state at 0.158 MeV, suggesting different L mixing and the participation of different configurations. Earlier cross-section work [26] showed surprisingly strong $L = 4$ mixing with the expected $L = 2$ transfer. The value of $R = G(4,3)/G(2,3)$ determined in the present work is -0.5 from A_{xx} data and -0.3 from A_{yy} data, which indicates that $L = 4$ is contributing

TABLE II. Values of R determined from minimizing χ^2 for angular distributions of A_{xx} and A_{yy} for the states studied in ^{56}Co and ^{46}Sc in comparison with theoretical shell-model predictions.

^{58}Ni$(d,\alpha)^{56}$Co					^{48}Ti$(d,\alpha)^{46}$Sc				
E_{ex} (MeV)	J^π	$R_{A_{yy}}$	$R_{A_{xx}}$	R_{th}	E_{ex} (MeV)	J^π	$R_{A_{yy}}$	$R_{A_{xx}}$	R_{th}
0.158	3^+	0.1	0.1	−0.4	0.228	3^+	0.0	0.0	−0.31
0.576	5^+	−0.2	−0.2	−0.15	0.774	5^+	0.1	0.1	−0.58
1.009	5^+	−0.2	−0.1	0.36	1.643	4^-	−0.1	+0.3	
1.930	3^+	−0.3	−0.5	−0.70	1.852	1^+	−1.0	−0.7	−0.33

significantly for this state, in agreement with an earlier finding [27]. A transfer involving only η_2 yields a value of $R=-0.32$ and is consistent with the observed ratio. The shell-model calculations including all the allowed configurations predict that the η_4 and η_2 configurations contribute most strongly to reactions populating this state, leading to a value of $R=-0.70$, an even stronger $L=4$ presence.

B. *L*-mixed transitions in the ^{48}Ti$(d,\alpha)^{46}$Sc reaction

Figure 4 shows the measured angular distributions of the cross section and TAP's for low-lying levels in ^{46}Ti obtained with 22-MeV deuterons. Excitation energies, spins, and parities for these levels were obtained from Ref. [28].

1. 3^+ level at 0.228 MeV

The angular distribution of the cross section for this level, shown in Fig. 4(a), resembles that of the 0.158-MeV level in ^{56}Co. The L mixing should therefore be quite similar. A pure $L=2$ transfer and predominant transfer for the η_1 configuration was suggested by Lewis [29] in his analysis of (d,α) cross-section angular distributions. Our fits to cross-section and TAP distributions show a χ^2 minimum for $R=G(4,3)/G(2,3)=0$, in agreement with this earlier work. The shell-model calculations predict the reaction to proceed mainly via η_1 and η_2, with a large spectroscopic amplitude for η_1, and yield $R=-0.31$, which is in reasonable agreement with our experimental result. If the only configuration considered were η_1, then $R(\eta_1)=-0.5$, suggesting that, for a closer agreement with the experiment, the spectroscopic amplitude for η_2 or η_3 should be larger.

2. 5^+ level at 0.774 MeV

Angular distributions of the cross section, VAP's, and TAP's for this state, shown in Fig. 4(b), are similar to those of the levels at 0.576 and 1.009 MeV in ^{56}Co, indicating that $L=4$ should be the dominant L transfer and η_2 an important configuration involved. This level has been identified as populated by $L=4$ transfer from cross-section measurements [29], although some evidence was seen for $L=6$. Our TAP angular distributions, shown in Fig. 4(b), were fit to yield $R=G(6,5)/G(4,5)=0.1$, as shown in Fig. 5. This disagrees with the shell-model calculation for low-lying states in ^{46}Sc, which predicts a major contribution from the η_1 configuration, leading to a value of $R=-0.58$. The χ^2 obtained from comparisons to VAP data for this transition shows little sensitivity to R, as shown in Fig. 5 for this state. This lack of sensitivity is typical of the VAP data taken as part of the present work.

3. 4^- level at 1.643 MeV

In earlier cross section work [29], this transition was analyzed as $L=3$ with a small $L=5$ admixture. The angular distributions for this state, shown in Fig. 4(c), show a strong $L=3$ pattern, consistent with the previous work, and a best fit for $R=G(5,4)/G(3,4)=-0.1$ for A_{yy} and $R=0.3$ for A_{xx}. Unlike all other transitions analyzed, the population of this state must involve the pick-up of particles from the *sd* and *fp* shells, probably including the configuration $\pi(1d_{3/2})\nu(1f_{7/2})$. A calculation assuming only the mentioned configuration yields $R=1.0$, in disagreement with our result. This indicates the need for a contribution from other *sd*-shell orbitals, and consequently a theoretical prediction of the mixing requires making shell-model calculations in a larger basis, including both *sd* and *fp* active shells.

4. 1^+ level at 1.852 MeV

Angular distributions for the transition to this state are quite different from those of the states previously discussed, but interestingly, we can observe a similarity to the angular distributions obtained in other 1^+ transitions [3], namely, in ^{36,38}Ar$(d,\alpha)^{34,36}$Cl and ^{32}S$(d,\alpha)^{30}$P reactions. They show a negative A_{xx} and a positive and constant A_{yy} with a value of approximately 0.85. This pattern is a clear indication that the L-mixing ratio has to be negative, as can be understood using the peripheral model [5]. In fact, in all the previous cases of transitions to 1^+ states, the $R=G(2,1)/G(0,1)$ values obtained from the fit to the observables were negative, in agreement with the shell-model predictions [3].

In this transition, the best fit to the angular distributions is obtained with a mixture of approximately equal amounts of $L=0$ and 2, leading to a best-fit value of $R=-0.9$, in agreement with a previous analysis of the cross-section angular distribution [29]. The calculated angular distributions corresponding to this value of R are shown in Fig. 4(d). Unlike the cross section, TAP's are quite sensitive to the sign of the mixing ratio. This can be seen in Fig. 8 where there is a plot of χ^2 as a function of R for $\sigma(\theta)$, A_{xx}, and A_{yy}. An interesting feature is the asymmetry between the two dips in χ^2 for the cross-section data shown in Fig. 8(b), which reflects the presence of spin-dependent distortions. The χ^2 minima are

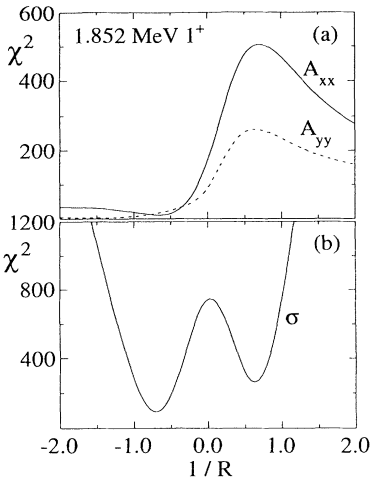

FIG. 8. χ^2 variations with R using cross-section and TAP data for the 1^+ state of ^{46}Sc at $E_x=1.852$ MeV.

not particularly pronounced for the TAP data of this transition, and cross-section data are needed to localize the value of R. Since there exists a large number of possible configurations which may contribute to this transition, shell-model calculations are more uncertain for this state at this energy. A calculation including all ten allowed configurations yields a value of $R=-0.33$. Although the calculation predicts a different magnitude from our experimental result, it does predict the sign of R suggested by the TAP pattern.

V. SUMMARY AND CONCLUSION

We have used tensor analyzing power angular distributions in (d,α) reactions to obtain both the magnitude and sign of the L-mixing ratios $R=G(L=J+1,J)/G(L=J-1,J)$. These were determined by systematically varying R to minimize differences between experimental and theoretical values of A_{xx} and A_{yy}. For all the states where fits were attempted, the χ^2 showed a pronounced minimum for A_{xx} and A_{yy} as a function of R, within the range of 0.4 and in most cases 0.1, as shown in Table II. These minima are reasonably stable to changes in optical-model potentials and the form factor for the deuteron bound state in the heavy system. The vector analyzing powers were found to have much less sensitivity to R, while cross-section angular distributions showed sensitivity to the magnitude of R in some cases but much less sensitivity to the sign. Shell-model calculations made for these transitions, based on active $1f_{7/2}$, $2p_{3/2}$, $1f_{5/2}$, and $2p_{1/2}$ orbitals, show that significant contributions are expected from three or more configurations for all the transitions studied. This makes it impossible to uniquely determine the relative magnitude and sign of each spectroscopic amplitude from the data, since the mixing ratio can provide such information only in the case of two predominant configurations. However, the value of the L-mixing ratio can serve as a test of the shell-model predictions of the magnitude and sign of the spectroscopic amplitudes. Hopefully, the present data will serve to help inspire new calculations.

In the present work, we have seen that states of the same J^π that are populated often have comparable angular distributions of cross sections, VAP's and TAP's. A simple explanation for the similarity of the distributions of the 5^+ states in both ^{56}Co and ^{46}Sc is that the same configurations are important in each transfer. Even more striking is the case of the 1^+ state in ^{46}Sc at 1.852 MeV. This strongly populated state has TAP angular distributions with large magnitudes for both A_{xx} and A_{yy}. The relatively large (≈ 0.85) and constant A_{yy} values observed for this transition are similar to measurements made for 1^+ states in ^{34,36}Cl and ^{30}P. Other cross-section and TAP angular distributions for these 1^+ states compare quite closely, suggesting that the dominant n-p pickup patterns are related, perhaps through the pickup of both particles from the same shells.

An additional conclusion from the present work is that the n-p transfer for (d,α) reactions in this mass region is dominated by $L=J-1$ transfer. There was strong dominance of $L=J-1$ for all states studied, except for the aforementioned 1^+ state in ^{46}Ti at 1.852 MeV. We do not speculate on the reason for this dominance which has been noted by others [30].

Finally, we have compared data to calculations using global OMP's for deuteron and alpha-particle potentials consistent with folding-model expectations. A realistic wave function for the α particle was included, which is important for the extraction of spectroscopic information from TAP observables. With no variation in the input to these calculations from those established in a previous analysis of the strongest state populated in the ^{58}Ni$(d,\alpha)^{56}$Co and ^{48}Ti$(d,\alpha)^{46}$Sc reactions [4], we have obtained very good agreement between the exact finite-range DWBA calculations and the present cross-section and TAP angular distributions. This serves to put this reaction on a firm basis as a reliable spectroscopic tool.

This research was supported in part by the U.S. Department of Energy, Division of Nuclear Physics, under the Grant No. DE-FG05-88ER40442 and by the Portuguese JNICT, under Project No. PMCT/CEN/388/90.

[1] N. K. Glendenning, *Direct Nuclear Reactions* (Academic Press, New York, 1983).
[2] F. D. Santos *et al.*, Phys. Rev. C **32**, 338 (1985).
[3] C. M Bhat, Y. Tagishi, E. J. Ludwig, and B. A. Brown, Phys. Rev. C **34**, 736 (1986).
[4] E. R. Crosson *et al.*, Phys. Rev. C **45**, R492 (1992).
[5] A. M. Eiró and F. D. Santos, J. Phys. G **16**, 1139 (1990).
[6] R. Schiavilla, V. R. Pandharipande, and R. B. Wiringa, Nucl. Phys. **A449**, 219 (1986).
[7] M. Haller *et al.*, Nucl. Phys. **A419**, 45 (1984).
[8] P. Schiemenz *et al.*, in *Proceedings of the 6th International Conference on Polarization Phenomena,* Osaka, edited by Mikondo *et al.* [J. Phys. Soc. Jpn. Suppl. **55**, 1056 (1986)].
[9] G. G. Ohlsen, J. L. Gammel, and P. W. Keaton, Jr., Phys. Rev. C **5**, 1205 (1972).
[10] H. Wessner *et al.*, Nucl. Instrum. Methods A **286**, 175 (1990).
[11] L. Holland, *Vacuum Deposition of Thin Films* (Chapman and Hall, London, 1984).
[12] E. R. Crosson, Ph.D. dissertation, University of North Carolina, 1992, available from University Microfilms International, 300 N. Zeeb Rd., Ann Arbor, Michigan 48106.
[13] M. Toyama and M. Igarishi, Computer code TWOFNR, 1972.
[14] F. Merz *et al.*, Nucl. Phys. **A489**, 399 (1988).
[15] B. C. Karp *et al.*, Nucl. Phys. **A457**, 15 (1986).
[16] N. K. Glendenning, At. Data Nucl. Data Tables **16**, 1 (1975).
[17] W. W. Daehnick, J. D. Childs, and Z. Vrcelj, Phys. Rev. C **21**, 2253 (1980).
[18] H. H. Chang *et al.*, Nucl. Phys. **A270**, 413 (1976).
[19] D. A. Goldberg and S. M. Smith, Phys. Rev. Lett. **29**, 500 (1972); D. A. Goldberg, S. M. Smith, and G. F. Burdzik, Phys. Rev. C **10**, 1362 (1974).
[20] E. R. Crosson *et al.*, Phys. Rev. C **47**, 2690 (1993).

[21] W. W. Daehnick *et al.*, Phys. Rev. Lett. **41**, 639 (1978).
[22] W. D. Rae *et al.*, Computer code OXBASH, Michigan State University Cyclotron Report No. 524, 1982.
[23] W. A. Richter *et al.*, Nucl. Phys. **A523**, 325 (1991).
[24] M. G. Van der Merwe, W. A. Richter, and B. A. Brown (unpublished).
[25] H. Junde *et al.*, Nucl. Data Sheets **51**, 1 (1987).
[26] M. J. Schneider and W. W. Daehnick, Phys. Rev. C **4**, 1649 (1971).
[27] H. Nann *et al.*, Phys. Lett. **109B**, 175 (1982).
[28] D. E. Alburger, Nucl. Data Sheets **49**, 237 (1986).
[29] M. B. Lewis, Phys. Rev. **184**, 1081 (1969).
[30] A. Guichard *et al.*, Nucl. Phys. **A164**, 56 (1971); R. M. Del Vecchio *et al.*, Phys. Rev. C **3**, 1989 (1971).